Optimum Path of a Flying Object with Exponentially Decaying Density Medium

Said Abbasbandy[a], Mehmet Pakdemirli[b], and Elyas Shivanian[a]

[a] Department of Mathematics, Imam Khomeini International University, Ghazvin, 34149-16818, Iran
[b] Department of Mechanical Engineering, Celal Bayar University, 45140 Muradiye, Manisa, Turkey

Reprint requests to S. A.; E-mail address: abbasbandy@yahoo.com

Z. Naturforsch. **64a,** 431 – 438 (2009); received September 1, 2008 / revised February 12, 2009

In this paper, a differential equation describing the optimum path of a flying object is derived. The density of the fluid is assumed to be exponentially decaying with altitude. The equation is cast in to a dimensionless form and the exact solution is given. This equation is then analyzed by homotopy analysis method (HAM). The results showed in the figures reveal that this method is very effective and convenient.

Key words: Homotopy Analysis Method; Minimization Path; Series Solution.
PACS numbers: 02.30.Mv; 02.60.Lj; 04.25.-g

1. Introduction

The homotopy analysis method [1, 2] is developed to search the accurate asymptotic solutions of nonlinear problems. This technique has been successfully applied to many nonlinear problems such as nonlinear vibration [3], nonlinear water waves [4], viscous flows of non-Newtonian fluids [5 – 7], nonlinear boundary flow and heat transfer [8], [9], Von kármán viscous flow [10], nonlinear fractal Riccati differential equations [11], Black-Scholes equations [12, 13] and many other subjects [14 – 21]. Especially, Liao [2] proved that the homotopy analysis method logically contains some other non-perturbation techniques, such as Adomian's decomposition method, Lyapunov's artificial small parameter method, and the δ-expansion method.

Drag forces are the major source of energy loss for objects moving in a fluid medium. Minimization of work due to drag force may reduce fuel consumption. Several assumptions can be made for this purpose. One way to minimize drag work may be to search for an optimum path. The drag force depends on the density of the fluid, the drag coefficient, the cross-sectional area and the velocity. If all parameters are taken as constant, then the minimum drag work path would be a linear path.

However, these parameters change during motion. A special case in which the density of the fluid is exponentially decaying with altitude is treated. For this special case, the remaining parameters are assumed to be constant. The equation is cast into a dimensionless form. Two dimensionless parameters of significant importance appear. One is the decay parameter affecting changes in density and the other is the height/distance ratio. The dimensionless differential equation is solved and an exact analytical solution is obtained. Using homotopy analysis method (HAM), exact solution and the HAM solution is contrasted. Results agree with each other.

Several applications of this study are possible. Aeroplanes and helicopters can follow the minimum drag path to reduce fuel consumption. Ballistic missiles can also be programmed to follow such an optimum path for reduction of rocket fuel. Space vehicles especially when they move in the atmosphere of planets may follow the optimum path for energy reduction. Although density variations are very small for water compared to air, the optimum path idea can be applied to routes of submarines also.

2. Differential Equation of the Path

In this section, the differential equation describing the minimum drag work path is derived. The drag force F_{D} for an object moving in a fluid medium is [22]

$$F_{\mathrm{D}} = \frac{1}{2}\rho A C_{\mathrm{D}} U^2, \tag{1}$$

where ρ is the density of the fluid medium, A is the cross-sectional area normal to the direction of move-

ment, C_D is the drag coefficient and U is the velocity of the moving object. In the special case treated, the density is assumed to be a function of altitude y^*, i. e. $\rho = \rho(y^*)$. The work due to drag force along an incremental path ds^* is

$$dW_D = \frac{1}{2}\rho(y^*)AC_D U^2 ds^*, \tag{2}$$

where $ds^* = \sqrt{dx^{*2} + dy^{*2}} = \sqrt{1+y'^{*2}}dx^*$ for cartesian coordinates. For a path starting from origin and ending at an altitude of h and distance R, the total work is

$$W_D = \frac{1}{2}\int_0^R \rho(y^*)AC_D U^2 \sqrt{1+y'^{*2}}dx^*. \tag{3}$$

If the temperature variations are assumed to be negligible, the density of air exponentially decays with altitude [23]

$$\rho = \rho_0 e^{-\alpha y^*}, \tag{4}$$

where $\alpha = g/RT$ (g gravity acceleration, R gas constant and T temperature, all assumed to be constants). The Euler-Lagrange equation is employed for minimizing the above functional [24]

$$\frac{\partial F}{\partial y^*} - \frac{d}{dx^*}\left(\frac{\partial F}{\partial y'^*}\right) = 0, \tag{5}$$

where $F = \rho_0 e^{-\alpha y^*} AC_D U^2 \sqrt{1+y'^{*2}}$. Substituting equivalent of F into (5) yields finally

$$y''^* + \alpha\left(1+y'^{*2}\right) = 0. \tag{6}$$

The boundary conditions for the problem are

$$y^*(0) = 0, \quad y^*(R) = h. \tag{7}$$

For universality of results, the equations may be cast into a dimensionless form. The dimensionless distance and altitude is

$$x = \frac{x^*}{R}, \quad u = \frac{y^*}{h}. \tag{8}$$

Equations (6) and (7) can now be expressed in terms of dimensionless quantities as follows

$$u'' + \varepsilon\left(1+\beta^2 u'^2\right) = 0, u(0) = 0, \quad u(1) = 1, \tag{9}$$

where

$$\varepsilon = \frac{\alpha R^2}{h}, \quad \beta = \frac{h}{R}, \tag{10}$$

and the prime denotes differentiation with respect to x.

3. Series Solution by Homotopy Analysis Method

We now consider the nonlinear differential equation with the boundary conditions (9) derived in section 2 and apply the homotopy analysis method [2] to get series solution of the problem. The equations are repeated below:

$$u'' + \varepsilon(1+\beta^2 u'^2) = 0, u(0) = 0, \quad u(1) = 1. \tag{11}$$

According to HAM, we assume that the solution of system (11), $u(x)$, can be expressed by the following set of base functions:

$$\{x^m | m = 1,2,3,\ldots\}, \tag{12}$$

in the form

$$u(x) = \sum_{n=1}^{+\infty} a_n x^n. \tag{13}$$

According to (11), we choose the linear operator

$$\mathcal{L}[\phi(x;p)] = \frac{\partial^2 \phi(x;p)}{\partial x^2}, \tag{14}$$

with the property

$$\mathcal{L}[c_1 + c_2 x] = 0, \tag{15}$$

where c_1 and c_1 are constants. Also, we define the nonlinear operator

$$\mathcal{N}[\phi(x;p)] = \frac{\partial^2 \phi(x;p)}{\partial x^2} + \varepsilon\left[1+\beta^2\left(\frac{\partial \phi(x;p)}{\partial x}\right)^2\right]. \tag{16}$$

It is straightforward that the initial approximation should be in the form $u_0(x) = x$ that satisfies the boundary conditions. Also, the general zero-order deformation equation is as follows:

$$(1-p)\mathcal{L}[\phi(x;p) - u_0(x)] = p\hbar\mathcal{H}(x)\mathcal{N}[\phi(x;p)], \tag{17}$$

with the boundary conditions

$$\phi(0;p) = 0, \quad \phi(1,p) = 1, \tag{18}$$

and the high-order deformation equation is

$$\mathcal{L}[u_m(x) - \chi_m u_{m-1}(x)] = \hbar\mathcal{H}(x)R_m(\vec{u}_{m-1}), \tag{19}$$

with the boundary conditions

$$u_m(0) = 0, \quad u_m(1) = 0, \tag{20}$$

where

$$R_m(\vec{u}_{m-1}) = \frac{1}{(m-1)!}\frac{\partial^{m-1}\mathcal{N}[\phi(x;p)]}{\partial p^{m-1}}\Big|_{p=0}, \quad (21)$$

and

$$\chi_m = \begin{cases} 0, & m \le 1, \\ 1, & m > 1. \end{cases} \quad (22)$$

From (16) and (21), we have

$$R_m(\vec{u}_{m-1}) = u''_{m-1}(x) + \varepsilon(1-\chi_m) + \varepsilon\beta^2 \sum_{j=0}^{m-1} u'_j u'_{m-1-j}, \quad (23)$$

where the prime denotes differentiation with respect to x. Now, the solution of the mth-order deformation (19) with considering (23) for $m \ge 1$ becomes

$$u_m(x) = \chi_m u_{m-1}(x) + \hbar \int_0^x \int_0^s \mathcal{H}(\tau) R_m(\vec{u}_{m-1})(\tau)\mathrm{d}\tau\mathrm{d}s + c_1 + c_2 x, \quad (24)$$

where the integral constants c_1 and c_2 are determined by the boundary conditions (20). According to the rule of solution expression denoted by (13) and from (19), the auxiliary function $\mathcal{H}(\tau)$ should be in the form $\mathcal{H}(\tau) = \tau^k$, where k is an integer. It is found that, when $k \le -1$, the solution of the high-order deformation (19) or (24) contains the terms $\ln(x)$ or $\frac{1}{x^s}(s \ge 1)$, which incidentally disobeys the rule of solution expression (13). When $k \ge 1$, the base x^2 always disappears in the solution expression of the high-order deformation (19) or (24), so that the coefficient of the term x^2 cannot be modified even if the order of approximation tends to infinity. Thus, we had to set $k = 0$, which uniquely determines the corresponding auxiliary function $\mathcal{H}(\tau) = 1$. Therefore from (24), we can obtain $u(x) \approx U_M(x) = u_0(x) + \sum_{m=1}^{M} u_m(x)$ by computing the $u_i(x)$'s and choosing best value of $\hbar$. As proved by Liao [2] this must be the approximate solution of the original nonlinear equation.

4. Results and Discussion

In this section we obtain some primary approximations from (24) and then choose proper $\hbar$ with the help of $\hbar$-curves and finally we present results graphically by considering different values for ε and β.

Using (24) primary approximations are as follow:

$$\begin{aligned} u_0(x) &= x, \\ u_1(x) &= \frac{1}{2}\hbar\varepsilon(1+\beta^2)x^2 + \left(-\frac{1}{2}\hbar\varepsilon - \frac{1}{2}\hbar\varepsilon\beta^2\right)x, \\ u_2(x) &= \frac{1}{3}\varepsilon^2\beta^2\hbar^2x^3(1+\beta^2) + \frac{1}{2}(\hbar\varepsilon + \hbar\varepsilon\beta^2 + \hbar^2\varepsilon \\ &\quad + \hbar^2\varepsilon\beta^2 - \varepsilon^2\beta^2\hbar^2 - \varepsilon^2\beta^4\hbar^2)x^2 \\ &\quad + \left(\frac{1}{6}\varepsilon^2\beta^2\hbar^2 + \frac{1}{6}\varepsilon^2\beta^4\hbar^2 - \frac{1}{2}\hbar\varepsilon - \frac{1}{2}\hbar\varepsilon\beta^2 \right. \\ &\quad \left. - \frac{1}{2}\hbar^2\varepsilon - \frac{1}{2}\hbar^2\varepsilon\beta^2\right)x, \\ &\vdots \end{aligned} \quad (25)$$

The mth-order approximation of $u(x)$ can be generally expressed by

$$U_M(x) = \sum_{m=0}^{M} u_m(x) = \sum_{n=0}^{M} \mu_{M,n}(\hbar)x^{n+1}, \quad (26)$$

where $\mu_{m,n}(\hbar)$ is a coefficient dependent on $\hbar$. Considering problem (11) reveals that the values of ε and β determine the nonlinearity of the equation. So, we continue the discussion in two parts as follows.

4.1. Weak Nonlinearity: Small Values of ε and β

The exact solution subject to the given boundary condition can be found by reduction of order. The final result is

$$u_{\text{exact}}(x) = \frac{1}{\varepsilon\beta^2} \cdot \ln\left[\cos(\varepsilon\beta x) + \frac{e^{\varepsilon\beta^2} - \cos(\varepsilon\beta)}{\sin(\varepsilon\beta)}\sin(\varepsilon\beta x)\right]. \quad (27)$$

The solution is expressed in terms of dimensionless parameters namely ε (parameter related to the decay of density) and β (final height over final distance). Depending on the numerical values of dimensional parameters, R and h, the dimensionless parameters may be small or large. Considering the exact solution shows that when $\varepsilon\beta \ge \pi$ the argument of the function $\ln[\,]$ is negative for some $x \in [0,1]$ therefore, in this case, it is not expected there exist a solution for problem (11).

Equation (26) is a solution of problem (11) with respect to x and auxiliary parameter $\hbar$. In order to determine $\hbar$ for the convergence of (26), we plotted the so-called $\hbar$-curves of $u'(0)$ and $u''(0)$ for different small

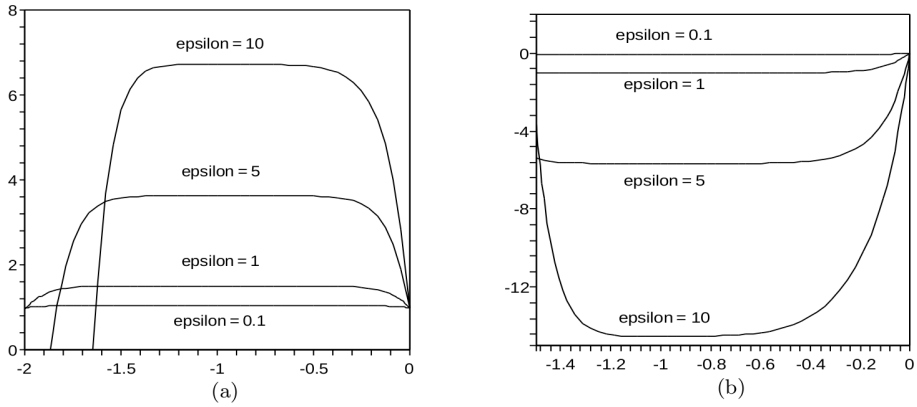

Fig. 1. (a) The $\hbar$-curves with $\beta = 0.1$ for $\varepsilon = 0.1, 1, 5, 10$, 10th-order approximation of $u'(0)$. (b) The $\hbar$-curves with $\beta = 0.1$ for $\varepsilon = 0.1, 1, 5, 10$, 10th-order approximation of $u''(0)$.

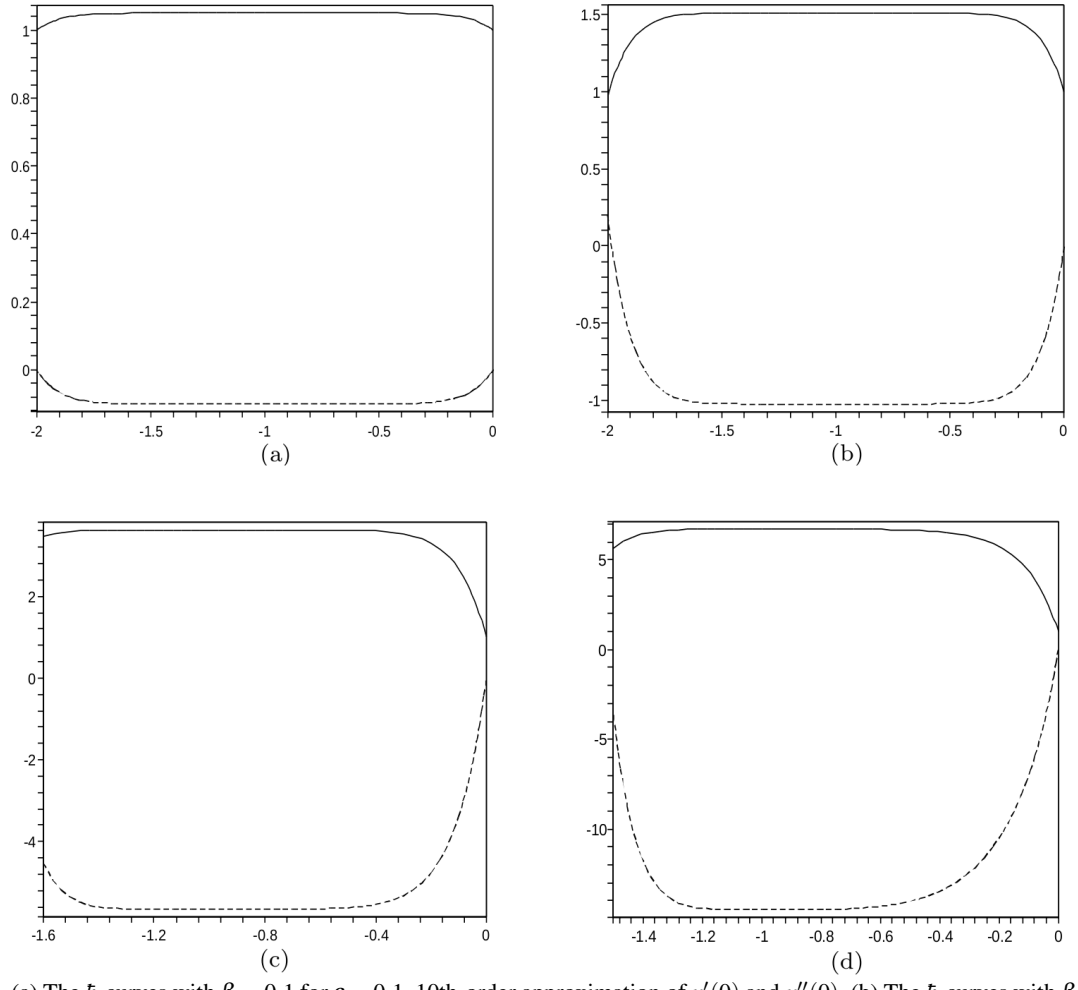

Fig. 2. (a) The $\hbar$-curves with $\beta = 0.1$ for $\varepsilon = 0.1$, 10th-order approximation of $u'(0)$ and $u''(0)$. (b) The $\hbar$-curves with $\beta = 0.1$ for $\varepsilon = 1$, 10th-order approximation of $u'(0)$ and $u''(0)$. (c) The $\hbar$-curves with $\beta = 0.1$ for $\varepsilon = 5$, 10th-order approximation of $u'(0)$ and $u''(0)$. (d) The $\hbar$-curves with $\beta = 0.1$ for $\varepsilon = 10$, 10th-order approximation of $u'(0)$ and $u''(0)$. Bold line: $u'(0)$, dashed line: $u''(0)$.

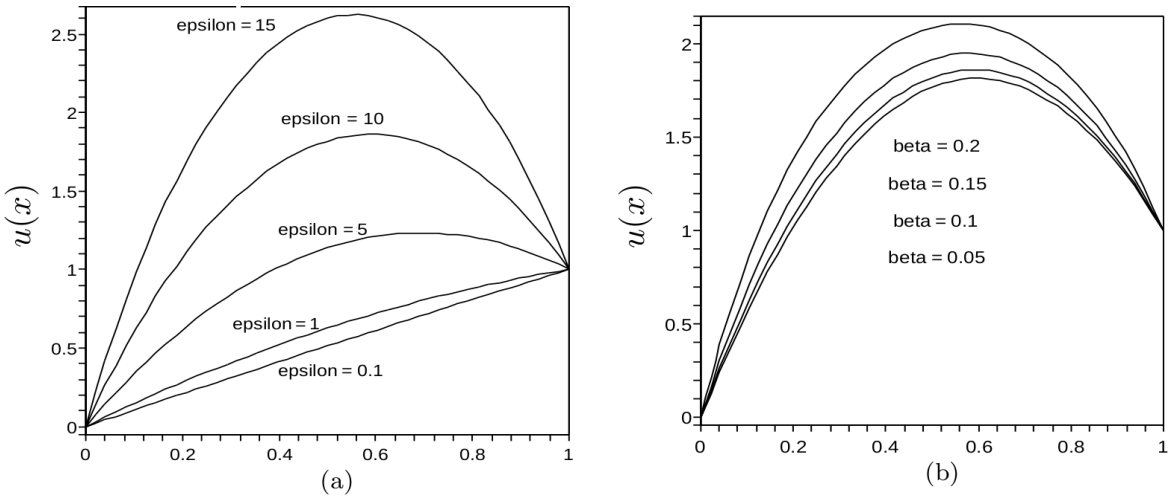

Fig. 3. (a) The 10th-order approximate solution for $\varepsilon = 0.1, 1, 5, 10, 15$ when $\beta = 0.1$. (b) The 10th-order approximate solution for $\beta = 0.05, 0.1, 0.15, 0.2$ from down to up, respectively, when $\varepsilon = 10$.

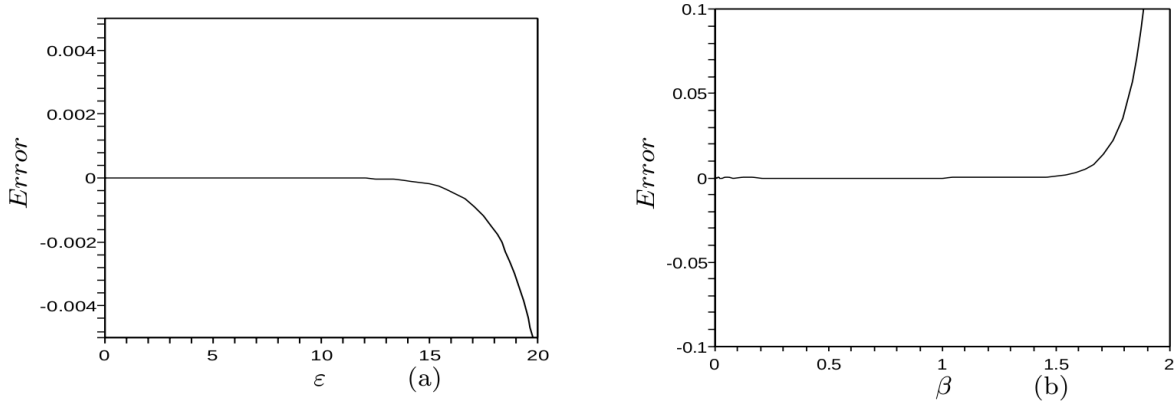

Fig. 4. (a) The error of 10th-order approximate solution corresponding to ε for $\beta = 0.1$ in $x = 0.5$. (b) The error of 10th-order approximate solution corresponding to β for $\varepsilon = 1$ in $x = 0.5$.

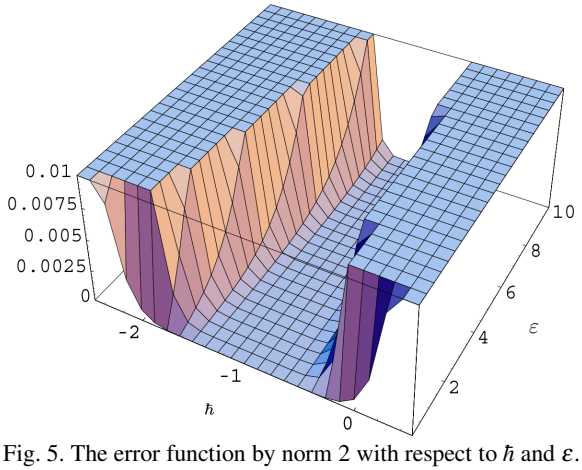

Fig. 5. The error function by norm 2 with respect to $\hbar$ and ε.

values of ε and β as shown in Figures 1 and 2. From these figures, it is easy to discover the valid region of $\hbar$. Therefore HAM can provide us with a convenient way to adjust and control the convergence region and rate of approximation series.

In Figure 1, $\hbar$-curves are shown with $\beta = 0.1$ and $\varepsilon = 0.1, 1, 5, 10$ for $u'(0)$ and $u''(0)$, respectively. Also, $\hbar$-curves of $u'(0)$ and $u''(0)$ are compared for $\varepsilon = 0.1, 1, 5, 10$ and $\beta = 0.1$ separately in Figure 2. As we can see, the valid region is in the vicinity of -1 therefore we can choose the well value for $\hbar$ from Figures 1 and 2 as -1. For this value of $\hbar$, the 10th-order approximate solution has been plotted in Figure 3, when $\varepsilon = 0.1, 1, 5, 10, 15$ for $\beta = 0.1$ and when $\beta = 0.05, 0.1, 0.15, 0.2$ for $\varepsilon = 10$.

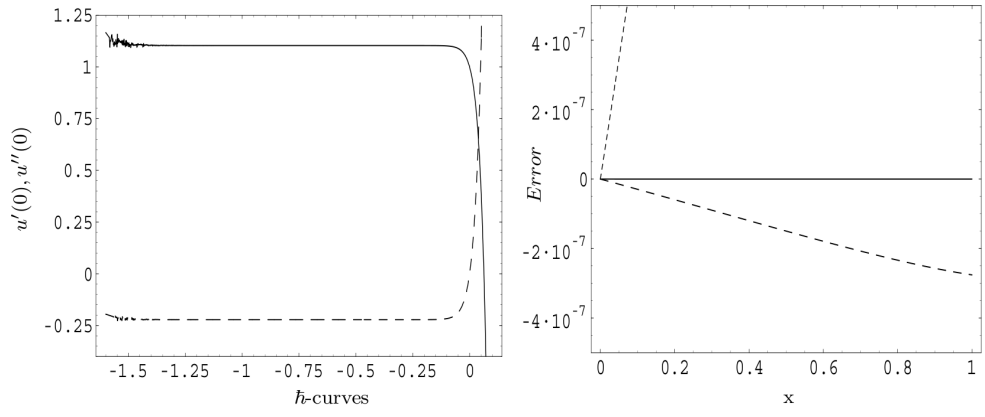

(a) (b)

Fig. 6. (a) The $\hbar$-curves with $\beta = 1$ and $\varepsilon = 0.1$ with 40th-order approximation. (b) The error of 40th-order approximate solution; bold line: $\hbar = -0.4$; dashed line: $\hbar = -0.8$; dotted line: $\hbar = -1$.

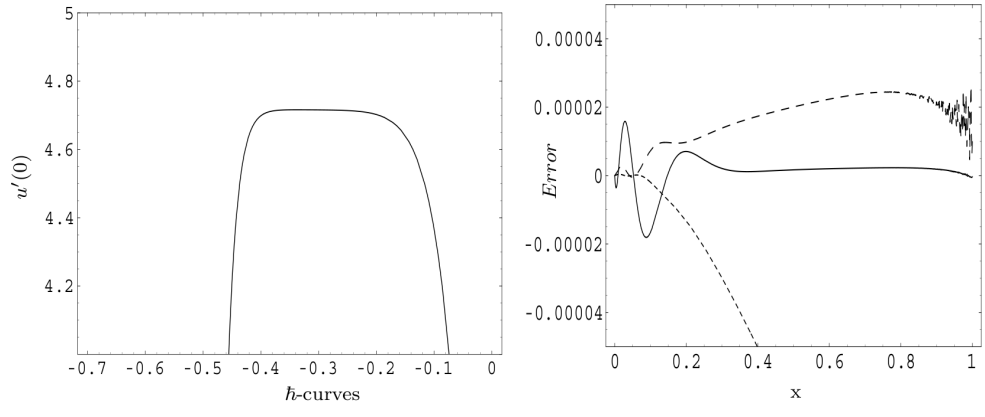

(a) (b)

Fig. 7. (a) The $\hbar$-curves with $\beta = 5$ and $\varepsilon = 0.1$ with 50th-order approximation. (b) The error of 50th-order approximate solution; bold line: $\hbar = -0.25$; dashed line: $\hbar = -0.30$; dotted line: $\hbar = -0.35$.

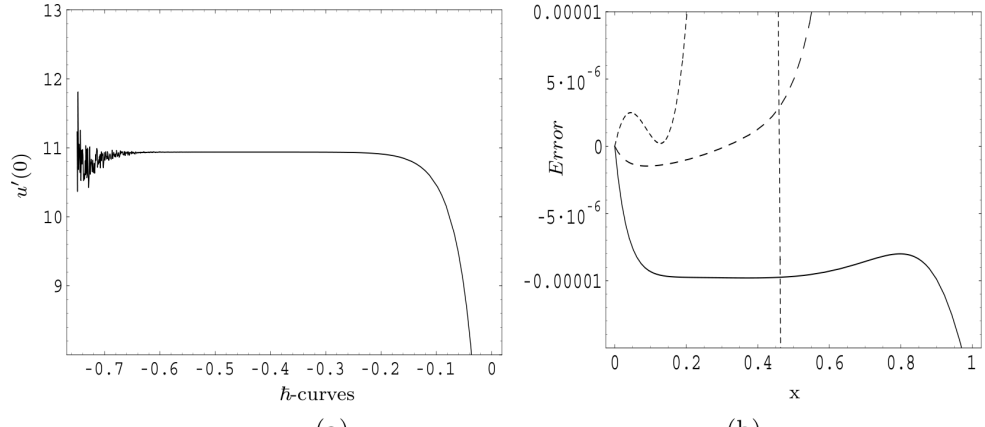

(a) (b)

Fig. 8. (a) The $\hbar$-curve with $\beta = 0.1$ and $\varepsilon = 15$ with 50th-order approximation. (b) The error of 50th-order approximate solution; bold line: $\hbar = -0.35$; dashed line: $\hbar = -0.40$; dotted line: $\hbar = -0.50$.

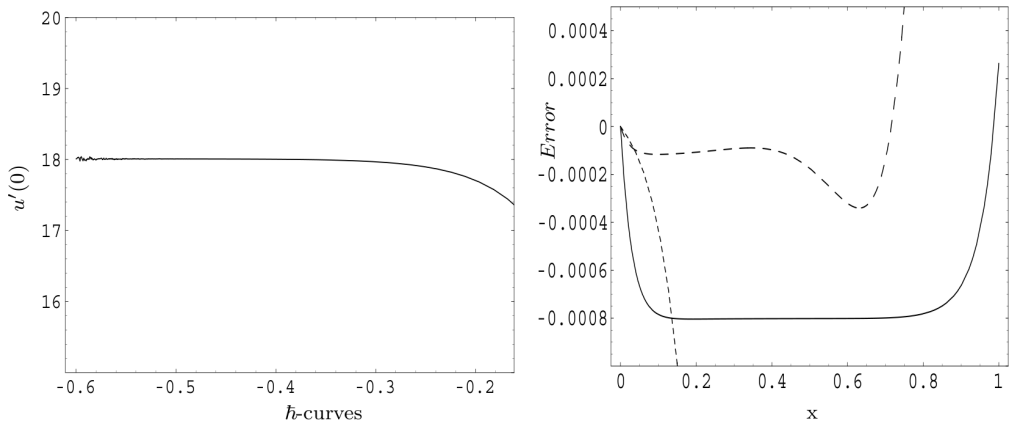

(a) (b)

Fig. 9. (a) (a) The $\hbar$-curve with $\beta = 0.1$ and $\varepsilon = 20$ with 50th-order approximation. (b) The error of 50th-order approximate solution; bold line: $\hbar = -0.32$; dashed line: $\hbar = -0.40$; dotted line: $\hbar = -0.50$.

Now, we want to compare the solution obtained by HAM with the exact solution. For this, in Figure 4(a), error function i. e. $u_{\text{HAM}} - u_{\text{exact}}$ in $x = 0.5$ corresponding to ε for interval $[0,20]$ is plotted for $\beta = 0.1$ and also, error function in $x = 0.5$ corresponding to β for interval $[0,2]$ is showed for $\varepsilon = 1$.

Also, to identify better values of $\hbar$, we plotted in Figure 5 the error of the approximate solution of 10th-order by norm 2, i. e.

$$\left[\frac{1}{10}\sum_{i=1}^{10}\left(u_{\text{HAM}}(x_i) - u_{\text{exact}}(x_i)\right)^2\right]^{\frac{1}{2}}, \tag{28}$$

where $x_i = 0.1i$, $i = 1,2,\ldots,10$ with respect to both of $\hbar$ and ε in $[-3,0]\times[0,10]$ for $\beta = 0.1$.

As we see in Figure 4, the error decreases with decrease of both ε and β at a fixed value of $x = 0.5$. Also, in Figure 5, the error decreases in vicinity of $\hbar = -1$ and especially when ε decreases.

4.2. Strong Nonlinearity: Large Values of ε and β

As mentioned earlier, homotopy analysis method can provide us with a convenient way to adjust and control the convergence region and the rate of approximation series. In this part, we show this is exactly right in spite of choosing values larger than in the previous part for ε and β.

We plotted $\hbar$-curves of $u'(0)$ and $u''(0)$ with 40th approximation for $\varepsilon = 0.1$ and $\beta = 1$ in Figure 6(a). It shows that the valid region for $\hbar$ is $[-1.4,-0.1]$ also. The error functions for different $\hbar$ are shown in Figure 6(b). As we see, it is clear that we can control the convergence of HAM series solution by convergence control parameter $\hbar$. Figures 6(a) and (b) are repeated in Figures 7(a) and (b) for $\varepsilon = 0.1$ and $\beta = 5$, obviously, in this case convergence of series solution can be controlled by choosing proper $\hbar$, too. Now, let us raise ε which leads to high nonlinearity of the problem (16). Consider $\beta = 0.1$ and $\varepsilon = 15$, the $\hbar$-curve of $u'(0)$ with 50th approximation is shown in Figure 8(a). It shows that the valid region of $\hbar$ is $[-0.6,-0.2]$ also. The error functions for different $\hbar$ are shown in Figure 8(b). As the same of previous cases, it is obvious that we can control convergence of HAM series solution by the convergence control parameter $\hbar$. Figures 8(a) and (b) have been repeated in Figures 9(a) and (b) for $\beta = 0.1$ and $\varepsilon = 20$. Furthermore, for a real comparison between the exact solution and the series approximate solution, we included Table 1 in case of strong nonlinearity of the problem which says up to how many decimal places the solution is comparable with the exact solution.

5. Conclusions

In this paper, the differential equation describing the optimum path of a flying object is derived. The density of the fluid is assumed to be exponentially decaying with altitude. The homotopy analysis method (HAM) [2] is applied to obtain the solution of this problem. HAM provides us with a convenient way to control the convergence of approximation series. Ap-

x	$\varepsilon = 0.1$ and $\beta = 5$		$\varepsilon = 20$ and $\beta = 0.1$	
	Exact Solution(8D)	$U_{50}(x)$ with $\hbar = -0.25$	Exact Solution(7D)	$U_{50}(x)$ with $\hbar = -0.32$
0.00	0.00000000	0.00000000	0.0000000	0.0000000
0.10	0.31122781	0.31121078	1.4553165	1.4545321
0.15	0.40667739	0.40667762	1.9856103	1.9848079
0.20	0.48347523	0.48348143	2.4194178	2.4186139
0.25	0.54766363	0.54766720	2.7722346	2.7714313
0.30	0.60274408	0.60274495	3.0547962	3.0539934
0.35	0.65092820	0.65092804	3.2746581	3.2738556
0.40	0.69370250	0.69370220	3.4371293	3.4363270
0.45	0.73211433	0.73211413	3.5458404	3.5450383
0.50	0.76692944	0.76692933	3.6030908	3.6022889
0.55	0.79872464	0.79872458	3.6100515	3.6092498
0.60	0.82794524	0.82794520	3.5668631	3.5660616
0.65	0.85494217	0.85494215	3.4726471	3.4718462
0.70	0.87999692	0.87999690	3.3254334	3.3246342
0.75	0.90333864	0.90333863	3.1219894	3.1211951
0.80	0.92515640	0.92515640	2.8575186	2.8567369
0.85	0.94560797	0.94560798	2.5251648	2.5244154
0.90	0.96482635	0.96482643	2.1152010	2.1145359
0.95	0.98292468	0.98292492	1.6136699	1.6132382
1.00	1.00000000	1.00000000	1.0000000	1.0000000

Table 1. Numerical results in case of strong nonlinearity of the problem.

proximate HAM solutions are compared with the exact solution. This work shows us the validity and great potential of HAM for nonlinear problems in science and engineering.

Acknowledgements

The authors would like to thank the anonymous referees for their constructive suggestions and comments.

[1] S. J. Liao, The proposed homotopy analysis techniques for the solution of nonlinear problems, PhD dissertation, Shanghai Jiao Tong University, 1992 (in English).
[2] S. J. Liao, Beyond Perturbation: Introduction to the Homotopy Analysis Method, Chapman Hall CRC/Press, Boca Raton 2003.
[3] S. J. Liao, Int. J. Non-Linear Mech. **39**, 271 (2004).
[4] S. J. Liao and K. F. Cheung, J. Eng. Math. **45**, 105 (2003).
[5] S. J. Liao, J. Fluid Mech. **488**, 189 (2003).
[6] H. Xu and S. J. Liao, J. Non-Newton. Fluid Mech. **129**, 46 (2005).
[7] H. Xu, S. J. Liao, and I. Pop, J. Non-Newton. Fluid Mech. **139**, 31 (2006).
[8] H. Xu, S. J. Liao, and I. Pop, Acta Mech. **184**, 87 (2006).
[9] H. Xu, S. J. Liao, and I. Pop, Eur. J. Mech. B: Fluids **26**, 15 (2007).
[10] H. Xu and S. J. Liao, Meccanica **41**, 599 (2006).
[11] J. Cang, Y. Tan, H. Xu, and S. J. Liao, Chaos, Solitons, and Fractals **40**, 1 (2009).
[12] S. P. Zhu, ANZIAM J. **47**, 477 (2006).
[13] S. P. Zhu, Quant. Finance **6**, 229 (2006).
[14] T. Hayat, S. Noreen, and M. Sajid, Int. J. Therm. Sci. **47**, 591 (2008).
[15] S. Abbasbandy, Nonlinear Dyn. **52**, 35 (2008).
[16] A. Mehmood, A. Ali, and T. Shah, Commun. Nonlinear Sci. Numer. Simul. **13**, 902 (2008).
[17] A. S. Bataineh, M. S. M. Noorani, and I. Hashim, Phys. Lett. A. **372**, 4062 (2008).
[18] T. T. Zhang, L. Jia, Z. C. Wang, and X. Li, Phys. Lett. A **372**, 3223 (2008).
[19] A. S. Bataineh, M. S. M. Noorani, and I. Hashim, Commun. Nonlinear Sci. Numer. Simul. **14**, 1121 (2009).
[20] S. Abbasbandy, Int. Commun. Heat Mass Tran. **34**, 380 (2007).
[21] S. Abbasbandy, M. Yürüsoy, and M. Pakdemirli, Z. Naturforsch. **63a**, 564 (2008).
[22] Y. A. Çengel and J. M. Cimbala, Fluid Mechanics, Fundamentals and Applications, McGraw Hill, New York 2006.
[23] E. L. Houghton and N. B. Carruthers, Aerodynamics for Engineering Students, Edward Arnold, London 1982.
[24] D. Zwillinger, Handbook of Differential Equations, Academic Press, San Diego 1989.